

Universidad Nacional Autónoma de México

Instituto de Radioastronomía y
Astrofísica

Evolution of the angular momentum during gravitational fragmentation of molecular clouds

Griselda Arroyo-Chávez

Advisor:

Enrique Vázquez-Semadeni



EXAMINATION COMMITTEE

1. Roberto Galván
2. Aina Palau
3. Alejandro Esquivel
4. Patrick Hennebelle
5. Lee Hartmann

MORELIA, MÉXICO, DECEMBER, 2021

TABLE OF CONTENT

INTRODUCTION- PAGE 03

Description of the angular momentum problem in molecular clouds and some of the proposed solutions

GOALS-PAGE 05

Objectives to be met to clarify the angular momentum transfer mechanism in molecular clouds from the GHC scenario

PENDING WORK-PAGE 15

Objetives to be met for the next semesters

GOALS COMPLETED-PAGE 06

How we measure and track angular momentum in particle sets in a hydrodynamic simulation for the first part of the project

COLLABORATIVE WORK-PAGE 17

Project that came out on the road

NEXT STEPS-PAGE 19

What is the plan for the next semester?

RESULTS AND DISCUSSION-PAGE 09

How the angular momentum evolves in sets of particles tracked in time and what consequences it can have

SCHEDULE-PAGE 18

Schedule of activities organized by semester for the tasks to be carried out during the PhD

REFERENCES-PAGE 20

INTRODUCTION

Angular momentum (AM) redistribution is a well-known phenomenon in systems such as accretion discs. However, the AM transfer mechanism is not fully understood at scales of molecular clouds (MC's). Ever since the first measurements of velocity gradients, and consequently of the AM in MC's, a systematic loss of AM has been observed over a wide range of scales, from tens of parsecs to fractions of parsec. Even the giant molecular clouds have a lower SAM value than their sur-

roundings (Imara and Blitz, 2011). One of the first interpretation was given by Fleck and Clark (1981), who interpreted this as the consequence of a turbulent cascade generated by the Galactic differential rotation. Then Goldsmith and Arquilla (1985) suggested that it was evidence of the AM loss during collapse and fragmentation of molecular clouds, with this AM being deposited in the orbital motions of the fragments. Nowadays this phenomenon is called as *Angular momentum problem* (AMP),

and is illustrated in Fig. 1, which shows the specific angular momentum (SAM) j vs radius R for a sample of molecular clouds, clumps and cores, which we have compiled from the sources indicated in the figure. A least squares fit to the data in this figure gives the expression

$$\frac{j}{\text{cm}^2 \text{ s}^{-1}} = 10^{22.7 \pm 0.002} \left(\frac{R}{1 \text{ pc}} \right)^{1.52 \pm 0.06},$$

which is represented by the black line in the figure. The associated 1σ error in the fitting parameters is indicated by the shaded region.

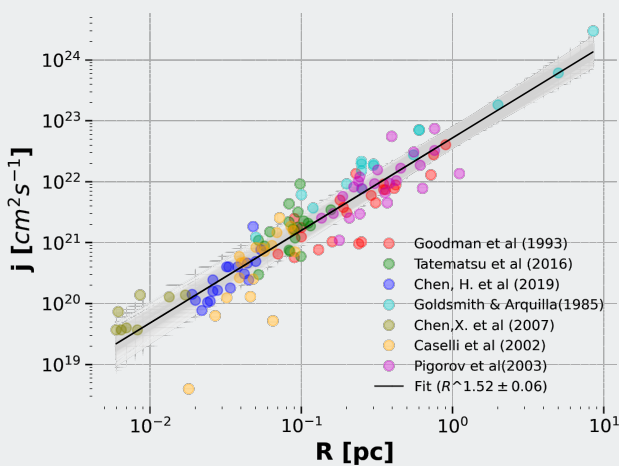


Figure 1: The observed j - R relation for molecular structures of sizes ~ 0.01 – 10 pc. The solid line represents the best fit. The set of light-gray lines represent the $1\text{-}\sigma$ error.

Spitzer (1978), and more recently Hennebelle et al. (2013), have discussed the AMP and how it would be impossible to form stars with a ratio of centrifugal to gravitational force of the order of 10^6 if the AM were conserved. Over the years different solutions have been proposed within the context of different models for MC's and star formation. Larson (1984) considered the possibility of torques produced by the turbulent viscosity, although he ruled it out under the argument that no mechanism was known which could sustain strong turbulence in the clouds. Thus, he instead proposed gravitational tidal torques between neighboring

density enhancements (“clumps”) as a mechanism to transfer AM among them.

Alternatively, the magnetic field was considered as another possible agent responsible for AM transfer. In particular, in the model of magnetically-supported clouds, with star formation mediated by ambipolar diffusion (see, e.g., the reviews by Shu et al., 1987; Mouschovias, 1991), the preferred mechanism to explain the redistribution of AM was magnetic braking (see the review by Bodenheimer, 1995, and references therein). Nevertheless, today it is known that this mechanism presents a series of problems, among them, the excessive removal of AM (Li et al., 2014) and the fact that the j - R relation develops also in non-magnetic simulations (e.g., Jappsen and Klessen, 2004).

Within the context of the so-called *gravoturbulent* scenario for MCs, Jappsen and Klessen (2004), similarly to Larson (1984), invoke gravitational torques as the mechanism responsible for transporting AM out of a clump. However, no clear evidence has been provided that AM redistribution occurs mainly via this mechanism in MCs.

More recently, Vázquez-Semadeni et al. (2019) have discussed a number of problems of the gravoturbulent scenario, and have suggested that molecular clouds and their substructures are all in a state of non-homologous gravitational contraction and fragmentation (e.g., Hartmann and Burkert, 2007; Vázquez-Semadeni et al., 2009, 2019; Ballesteros-Paredes et al., 2011; Ibáñez-Mejía et al., 2016); that is, in a regime of global, hierarchical collapse (GHC). However, the ori-

gin of the observed j - R scaling and the AM transfer mechanism has not been investigated within the context of the GHC scenario. In this sense, it is necessary to determine the importance of gravity in both problems, as well as in the development of other trends also observed in MCs when investigating their velocity gradients. This is the main objective of this work.

On smaller scales, in addition to reporting a depen-

dency $j \sim R^{1.6}$ for a sample of dense cores, Goodman et al. (1993) gave an analytic derivation for the relation j - R , assuming that *i*) the ratio β of rotational to gravitational energy was constant for all cores, *ii*) a linewidth-size scaling relation of the form $\sigma \propto R^{1/2}$ (Larson, 1981) holds for the cores, and *iii*) the cores are in approximate virial equilibrium.

Recently, in a Master's Degree research project (Arroyo-Chávez, 2020, hereinafter A20), we investigated the evolution of the SAM of a few clumps within a molecular cloud in an SPH numerical simulation of the formation and evolution of clouds within the warm diffuse neutral medium. To understand the mechanism that produces the apparent loss of angular momentum observed in regions of progressively smaller sizes, "clumps" were defined at a certain time t_{def} as connected sets of particles, and their evolution was followed both from the past ($t < t_{\text{def}}$) and toward the future ($t > t_{\text{def}}$). The time tracking was performed either as "lagrangian" sets of SPH particles (i.e., considering always the same set of particles), or as connected sets of particles above a certain density threshold, so that the constituent particles of the clump can change over time.

In this study, it was found that the evolution of j for clumps defined as lagrangian sets of particles and followed from the past presents two periods: an early one, in which the clumps evolve along the locus of the observational j - R diagram while they contract, and a late one, in which they evolve with $j \sim \text{cst.}$ during the contraction. Therefore, the evolution of the clumps in the

j - R diagram is reminiscent of the observed radial j profile on accretion disk scales (e.g., Pineda et al., 2019; Gaudel et al., 2020). It was furthermore found that the evolution along the observational locus occurs when the volume containing the particles belonging to the lagrangian set contained a large number of non-member particles, while the *cst.-j* stage occurred when this volume contains relatively few non-member particles.

On the other hand, when the lagrangian clumps were tracked to the future, it was found that they do not remain coherent. Instead, the innermost regions of the clumps collapse and form sinks (stellar particles) while the outer parts disperse, similarly to the process thought to occur in accretion disks. This result suggests that the observed j - R relation is the consequence of a *gravitational fragmentation* process in the clumps such that, if they are globally dominated by gravity, the clump sub-regions that give up AM to their neighbors can contract gravitationally, while the regions that gain AM are dispersed. The AM transfer mechanism appears to be turbulent viscosity, as indicated by the coexistence of non-member particles within the volume containing the lagrangian-set member particles. Furthermore,

assuming that the fragmentation and subsequent collapse must be such that at all times β remains approximately constant, according to the GHC scheme, in which gravitational energy is the source of the rest of energies, it was possible to extend the classic prediction between j and R , replacing it with the prediction that $j \propto \Sigma^{1/2} R^{3/2}$.

In A20, the previous results were obtained for only a few randomly selected clumps that satisfied only a few criteria of realism, and so it remained pending to confirm whether the observed behaviors are general trends rather than casual occurrences. This leads to questions such as: Are the observed trends global? What is the relative importance of gravity and turbulence in the production of the observed j - R relation? Moreover, since the study was performed with a non-magnetic simulation, while magnetic braking has been traditionally invoked in the resolution of the AMP, an important remaining question is what is the role of the magnetic field in the production of the observed relation? These questions led to the main objectives of the PhD project, which are listed below. Some of them have already been completed, while others are currently in process.

Goals

The goals to be met for this project are the following. The item marked with a check mark has been completed. Items marked with an ellipsis are under development and only a few initial ideas have been raised. The unmarked items are still pending.



- 1 Extend the study of A20 to a statistically significant sample of clumps and particle sets in order to establish the generality of the results.



- 2 Generate an analytical model for estimating the upper bound on star formation efficiency assuming that all structures are dominated by gravity and have an approximately constant rotational to gravitational energy ratio β .



- 3 Generate clump samples of large dynamic range in column density in both simulations and observations to test the predicted dependence in column density.

Preliminary calculations and measurements performed

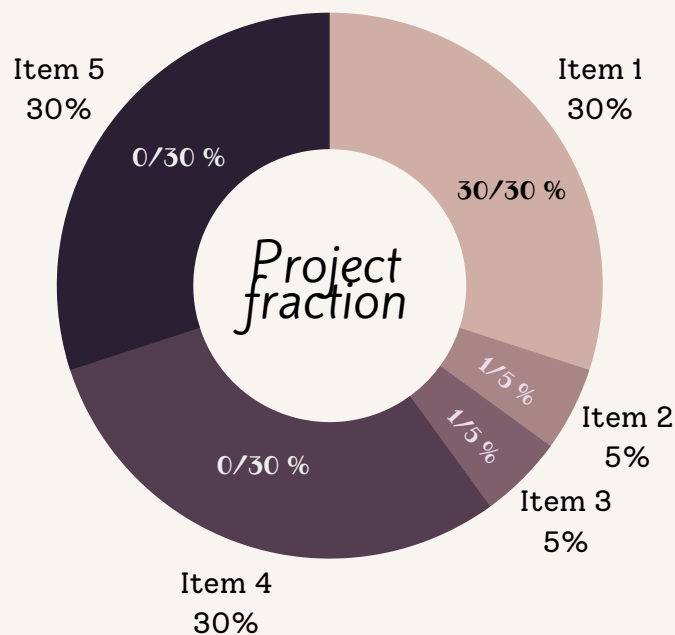


- 4 Investigate the precise role of gravity in the generation of the j - R relation, the constancy of β , and the AM transfer mechanism by measuring it in simulations without self-gravity.



- 5 Investigate the role of the magnetic field by repeating the study of Arroyo-Chávez and Vázquez-Semadeni (2021, in press, hereafter AV21) in MHDSFH simulations using the code Phantom.

Each of these goals represents a certain fraction of the overall project. This fraction is represented by the percentages in the diagram below. The percentage inside represents the progress of the specified goal.



Goals completed

Extension of the study by A20

All the results presented for this first part of the PhD project can be consulted in more detail in our article accepted for publication in ApJ (Arroyo-Chávez and Vázquez-Semadeni, 2021).

Among the goals stated above, the first part of the project, which includes items 1-3, focuses on understanding the mechanism that gives rise to the observed j - R scaling, as well as on the implications that this mechanism has on the fragmentation of progressively denser structures. During the first half of the PhD project, we focused on complying with item 1, of extending the results from A20 to a statistically significant sample, and refining the measurement methods. From the same simulation analyzed in A20, we produced a much more numerous numerical sample of clumps, using more rigorous selection criteria, both at a few isolated temporal snapshots to generate the j - R plot and at successions of times to investigate the evolution of the AM in the clumps. We also wrote the full AM conservation equation for fluids and added a discussion on their interpretation and applicability in our simulation. Based on the latter, on the expansion of the sample of tracked clumps, and on the evidence found in A20 that AM is lost through interaction with non-clump particles, we provide clearer support for our proposal that AM is transported by turbulent viscous torques. We now address these points in detail below.

Understanding the sources of angular momentum in molecular cloud scales

As part of the work carried out, and prior to the methodology followed for the study of the AM in MCs, we wrote the equation governing the evolution of the AM of a fluid parcel (with respect to some coordinate origin, e.g. the clump's center of mass) in order to understand the possible sources of AM represented by the active torques on the parcel. Let V be the volume of the parcel. By taking the cross product of the momentum conservation equation with the position vector r and integrating over V we have:

$$\begin{aligned}
 \int_V r \times \frac{\partial(\rho u)}{\partial t} dV = & - \int_V r \times \nabla \cdot (\rho u u) dV - \int_V r \times \nabla P dV - \int_V r \times \rho \nabla \phi dV \\
 & + \int_V r \times \mu (\nabla^2 u + \nabla \nabla \cdot u) dV + \int_V r \times \frac{1}{4\pi} (\nabla \times B) \times B dV.
 \end{aligned} \tag{1}$$

“Hydrodynamic” or “turbulent”
Pressure gradient
Gravitational

On the right hand side of eq. (1), we have the possible sources of torques that act on the fluid parcel, which are indicated by arrows. On the scales of molecular clouds and their fragments, magnetic (Bodenheimer, 1995) or gravitational torques are usually invoked as the likely mechanism responsible for AM transfer (Jappsen and Klessen, 2004; Kuznetsova et al., 2019), rather than viscous or pressure-gradient or hydrodynamic torques (from the advective term of the moment equation). Viscous torques are discarded because the molecular viscosity is negligible, while turbulent (or “eddy”) viscosity torques are neglected probably because of the argument by Larson (1984) that no sources of energy were known at the time to sustain a significant levels of turbulence. However, we know today that molecular clouds are clearly turbulent, so both the term pressure gradient and hydrodynamic torques or ram pressure should not be discarded.

In addition, Hennebelle et al. (2013) have pointed out (see their equation [4.12]) that the turbulent-torque term is an internal AM transport term so that globally AM is conserved. However, this term does not prevent the exchange of AM between fragments or within them, so that the net effect is that some regions gain AM an others lose it. In the following sections we will show some results from AV21 that appear to support this scenario.

The simulation

We analyzed an SPH simulation of decaying turbulence that was performed with the code GADGET-2, using $296^3 \approx 2.6 \times 10^7$ particles in a box of 256 pc per side (Heiner et al., 2015). The mass per particle was set at $0.06M_{\odot}$, thus the total mass in the numerical box is $1.58 \times 10^6M_{\odot}$. The initial density and temperature were set at $n(t=0) = 3 \text{ cm}^{-3}$ and $T(t=0) = 730 \text{ K}$, respectively. In this version of the code, the prescription for sink particles from Jappsen et al. (2005) was used, setting the density threshold for sink particle formation at $3.2 \times 10^6 \text{ cm}^{-3}$. The cooling and heating functions from Koyama and Inutsuka (2002), with the topographical correction given by Vázquez-Semadeni et al. (2007) were also used. For the studies carried on in this work, we selected snapshots between times 15.23 and 15.94 (see Fig. 2) Myr, at which there are already enough dense structures formed.

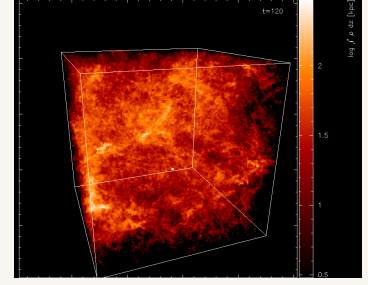


Figure 2: Simulation at $t = 15.94$ Myr.

Clump definition and numerical sample

We initially defined clumps using the algorithm introduced in Camacho et al. (2016), where “connected” SPH particles (i.e., particles within the smoothing lengths of each other) above some specific density threshold are associated to a clump around a local maximum of density. Because we are also interested in the evolution of the AM, some randomly selected clumps were tracked in time. We refer to these tracked clumps as “sets” of particles, since some types of tracking implemented later do not agree with the traditional definition of a clump as a connected overdensity.

We selected four timesteps in the simulation after the formation of the first sink ($t = 14.74$ Myr) to determine the j - R relation of a sample of clumps collected over the entire numerical box and at various times. The timesteps correspond to $t = 17.92$, $t = 19.92$, $t = 23.24$ and $t = 25.23$ Myr. We applied the clump-finding algorithm at these times with thresholds $n_{\text{th}} = 10^3$, 3×10^3 , 10^4 , 3×10^4 , and 10^5 cm^{-3} , rejecting those clumps with

less than 60 particles (1.5 times the number of particles within the smoothing radius) in order to guarantee that the retained ones are sufficiently resolved (Bate and Burkert, 1997).

Furthermore, since the simulation does not include any form of feedback we also restrict our sample to clumps whose star formation efficiency (SFE) satisfies

$$\text{SFE} \equiv \frac{M_*}{M_* + M_{\text{gas}}} < 30\%, \quad (2)$$

where M_* is the mass in stars (sinks). A sink will be associated with a clump if it is within the box defined by the minimum and maximum values of the positions of the clump particles on the three coordinate axes (see Fig. 3).

On the other hand, for the clumps tracked over time, we used two different approaches. In one of them, we considered a few randomly-chosen clumps from the full sample, and followed the (fixed) set of their constituent particle both from the past and towards the future of the time t_{def} at which the sets were defined. We refer to these as *la-*

grangian SPH particle sets. The tracking from the past was carried out over 2.65 Myr. The tracking to the future was carried out only until the last snapshot before a sink formed within the particle set. The second approach was the traditional one, in which we defined the clumps as connected overdensities at all times during the tracking. In this case, the set of particles making up the clump varied over time. Table 1 shows the properties of the 18 sets tracked. For comparison, in A20 there were only 7 of these clumps.

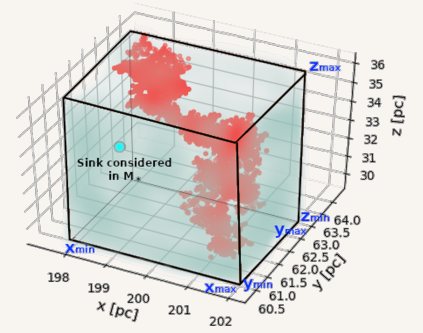


Figure 3: Parallelepiped defined by the minimum and maximum coordinates along each axis of the SPH particles belonging to the clump (red dots).

Estimation of size and j

For the size estimation we used different approaches for the clumps defined at a single time to measure the j - R relation, and for those that were tracked over time. For the former, where the particles are connected, we calculated the radius of a clump as that of a sphere with the same volume; i.e., $R = (3V/4\pi)^{1/3}$. In turn, for a discrete set of SPH particles, the total volume V was calculated as (Camacho et al., 2016)

$$V = \sum_{i=1}^{N_c} V_i = \sum_{i=1}^{N_c} \frac{m_p}{\rho_i} = m_p \sum_{i=1}^{N_c} \rho_i^{-1}, \quad (3)$$

where V_i is the volume of each particle.

For the case of the tracked lagrangian sets, because at some time t different from the definition time the particles will in general be more dispersed, and the volume they subtend will contain other “intruder” particles that do not belong to the tracked set, eq. (3) does

not reflect the real spatial extension of the set. In this case, the radius of the clump was determined as the geometric average of half the maximum difference in position of the constituent particles along each of the coordinate axes that is, as

$$R \approx \left(\frac{x_{max} - x_{min}}{2} \times \frac{y_{max} - y_{min}}{2} \times \frac{z_{max} - z_{min}}{2} \right)^{1/3}. \quad (4)$$

Once the radius had been estimated, the AM of each clump was calculated from the position and velocity vectors of the SPH particles with respect to its own center of mass, so that

$$\mathbf{J} = \mathbf{r}_{CM} \times \mathbf{p}_{CM} = \mathbf{r}_{CM} \times m_p \mathbf{v}_{CM}, \quad (5)$$

where the subscript CM represents quantities measured with respect to the clump’s center of mass. In this way, the SAM will be simply given by $j \equiv \mathbf{J}/M_{gas}$.

Table 1. Characteristics of clumps tracked over time

Name	t_{def} (Myr)	n_{th} (cm ⁻³)	Type		Tracking	
			Lagrangian set	Conected clump above n_{th}	From past ($t < t_{def}$) to present ($t = t_{def}$)	From present ($t = t_{def}$) to future ($t > t_{def}$)
C1	19.92	10 ³	X		X	
C2	19.92	3 × 10 ³	X		X	
C3	19.92	10 ⁴	X		X	
C4	19.92	3 × 10 ⁴	X		X	
C5	19.92	10 ⁵	X		X	
C6	25.23	10 ³	X		X	
C7	25.23	3 × 10 ³	X		X	
C8	25.23	10 ⁴	X		X	
C9	25.23	3 × 10 ⁴	X		X	
C10	25.23	10 ⁵	X		X	
C11	17.26	10 ³	X			X
C12	19.92	3 × 10 ³	X			X
C13	19.92	10 ⁴	X			X
C14	23.24	3 × 10 ⁴	X			X
C15	23.24	10 ³	X			X
C16	17.26	3 × 10 ³		X		X
C17	17.93	3 × 10 ³		X		X
C18	17.93	3 × 10 ³		X		X

t_{def} : definition time; n_{th} : definition threshold density

RESULTS AND DISCUSSION

j - R relation for the full numerical clump sample at fixed times

Figure 4 shows the j - R relation for the complete sample of clumps obtained from four different times of the simulation and with the five density thresholds selected, with the radius R calculated from the clump’s volume according to eq. (3). In this figure, the different colors correspond to the density threshold used to define clumps, and the different symbols denote the clump definition time, t_{def} . The red line represents a least-squares fit to the data for the numerical sample, given by

$$j = 10^{22.9 \pm 0.03} \left(\frac{R}{1 \text{ pc}} \right)^{1.52 \pm 0.06} \text{ cm}^2 \text{ s}^{-1}, \quad (6)$$

while the black line shows the fit to the observational sample shown in Fig. 1. From this fitting it can be seen that the numerical sample exhibits a slope and intercept remarkably close to those of the observational sample, suggesting that the GHC simulation is capable of accurately reproducing AM redistribution in MCs.

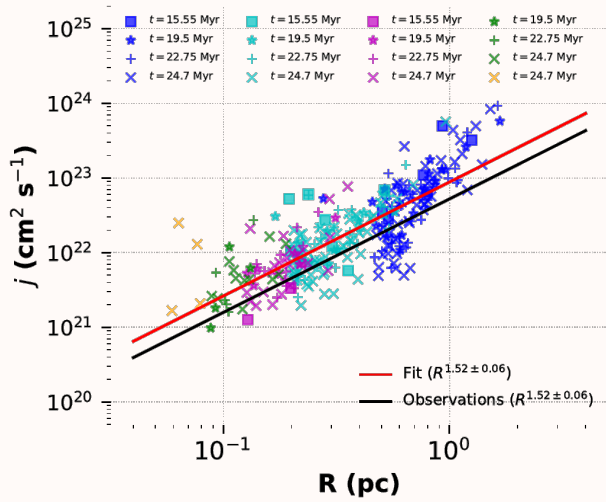


Figure 4: The j - R relation for the numerical clump sample, considering clumps defined as connected regions above a density threshold: $n_{\text{th}} = 10^3$ (blue), 3×10^3 (cyan), 10^4 (magenta), 3×10^4 (green), and 10^5 cm^{-3} (yellow), at different times. The black line represents a fit to the observations (Fig. 1), while the red line denotes a fit to the numerical sample.

j evolution for lagrangian particle sets

Tracking nested sets from the past

From Table 1 it can be seen that 15 of the 18 selected clumps are lagrangian sets. Clumps

C1-C5 correspond to a single structure seen with different density thresholds, with C1 being the largest and most diffuse structure that encloses the other, denser regions. The evolution of each lagrangian set in the j - R diagram over the 2.65 Myr prior to t_{def} (19.92 Myr) is shown in Fig. 5. In this figure, the clumps evolve from right to left, the colors correspond to different density thresholds, and the vertical lines indicate the time at which a change in the slope of the evolutionary track occurs for the lagrangian set of the corresponding color. The red filled square at the extreme left of each track corresponds to t_{def} , which in this case is the *final* time. The black line represents the fit to the observational data from Fig. 1. For the three smallest particle sets, two main periods of evolution can be identified: an early period in which the evolutionary track has a slope similar to that of the observational relation, and a late one over which j remains approximately constant. The transition to $j \sim \text{cst.}$ occurs when the clump is already quite compact. The period of AM loss occurs when the lagrangian set of particles is very scattered, and presumably with many “intruders”. This leads to the following

Hypothesis

The member particles can transfer their AM to the intruders, and thus become capable of contracting.

In order to test this hypothesis, we defined a “minimal rectangular box” as a rectangular volume enclosing the lagrangian set at each time as in Fig. 3, and determine the fraction of intruder particles in this volume. In order to not overestimate the number of intruders due to the geometry of the sets—that is, if they are particularly elongated in a certain direction—we consider the ratio of the number of intruder particles within the minimal box at time t , $N(t)$, to the number of intruders within the corresponding minimal box at the final time ($N(t_{\text{def}})$). Figure 6 shows the evolution of this ratio for the five lagrangian sets considered. The colored vertical lines represent the time at which the slope of the evolutionary track for each clump in Fig. 5 changes, if it does. Note that the green line coincides with the yellow line, and thus it is not visible. The vertical red dotted line indicates the definition time, t_{def} .

Figure 6 shows that, on average, the particle sets exhibiting an evolutionary track segment parallel to the observational slope in the j - R diagram (yellow, green and purple lines) had in the past few Myr a normalized intruder fraction larger than three times the value at the final time. Instead, the clumps that do not exhibit such stage (blue and cyan lines) had an initial value of this ratio at most twice the final value. This

result supports the hypothesis that a lagrangian set of SPH particles can lose AM as long as it has a companion set of particles to transfer it to, and instead evolves at roughly constant j when it is evolving mostly as an isolated entity. Also, this argues against the dominant torques being gravitational, since these would require the existence of nearby density *enhancements* capable of producing tidal stresses on the clump, while here the exchange appears to be with the immediate neighbors within the *same* clump. This therefore appears much more related to the mechanism of turbulent viscosity

(see the “Analytical estimates” section).

We performed a similar study for clumps C6-C10, which were also defined at different density thresholds, but correspond to spatially independent, rather than nested structures. These clumps exhibit a similar trend to those in Fig. 5, suggesting that this behavior is general, and not just an incidental property of the parent structure to which clumps C1-C5 belong (for details see Arroyo-Chávez and Vázquez-Semadeni, 2021).

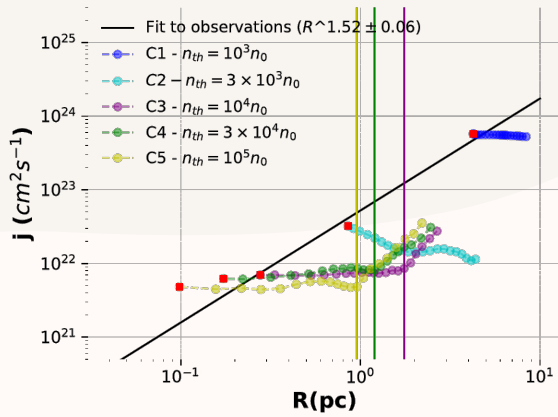


Figure 5: Evolutionary tracks from the past (since $t = 17.27$ Myr) up to $t_{\text{def}} = 19.92$ Myr for the five lagrangian sets C1-C5. The lagrangian sets evolve from right to left in this diagram, with the red filled square representing the final time, t_{def} . The vertical lines mark the radius of each set at which its track changes slope, with their color indicating their corresponding lagrangian set. The black line represents the fit made to the observational sample shown in Fig. 1.

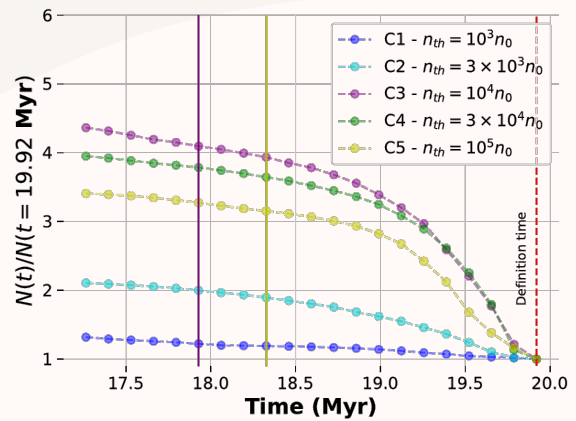


Figure 6: Ratio of the number of intruder particles within the minimal rectangular box that encloses each of the lagrangian sets C1-C5 at the indicated time t to the number of intruders at $t = t_{\text{def}}$. The solid vertical lines represent the time at which the slope of the corresponding evolutionary track in Fig. 5 changes.

Tracking independent sets to the future

We are interested in knowing both where AM comes from and where it goes in molecular clouds and their substructures. As a complement to the tracking backwards, we have tracked five lagrangian sets (C11-C15 in Table 1) to the future. For these, we study not only the j - R relation, but also how the sets evolve spatially in relation to the redistribution of AM. The spatial distribution and density evolution for these clumps is shown in Fig. 7. It can be seen that, as time proceeds, some of the member particles of clumps C11-C14 appear to *disperse* (red dots), others are involved in a local collapse, becoming denser and much more compact (cyan, blue and purple dots). Regarding clump C15, it is seen that the entire set of particles disperses, indicating that this is an example of a transient, dispersing clump.

It can also be seen that a fraction of the member particles reduces its density to values below the definition threshold and appear to disperse from the clump, in spite of having been initially all above the threshold density. We have observed this phenomenon in all sets of particles tracked to the future that develop a collapse center. *This suggests that losing a fraction of the clump’s mass to carry away the AM is a necessary condition for the rest of the clump to be able to collapse*, in a manner similar to the process of disk accretion towards a central object.

To test for this, we measured the SAM of the densest (innermost) and the most diffuse (ouertmost) regions of

the clumps (see Figure 8), finding that the regions with the highest SAM are precisely the least dense ones in the periphery of the clump, which are acquiring AM to later disperse. Conversely, the centermost regions have the least AM, and are in the process of further losing it. AM transfer in a clump can then be viewed as layered transmission similar to an accretion disc.

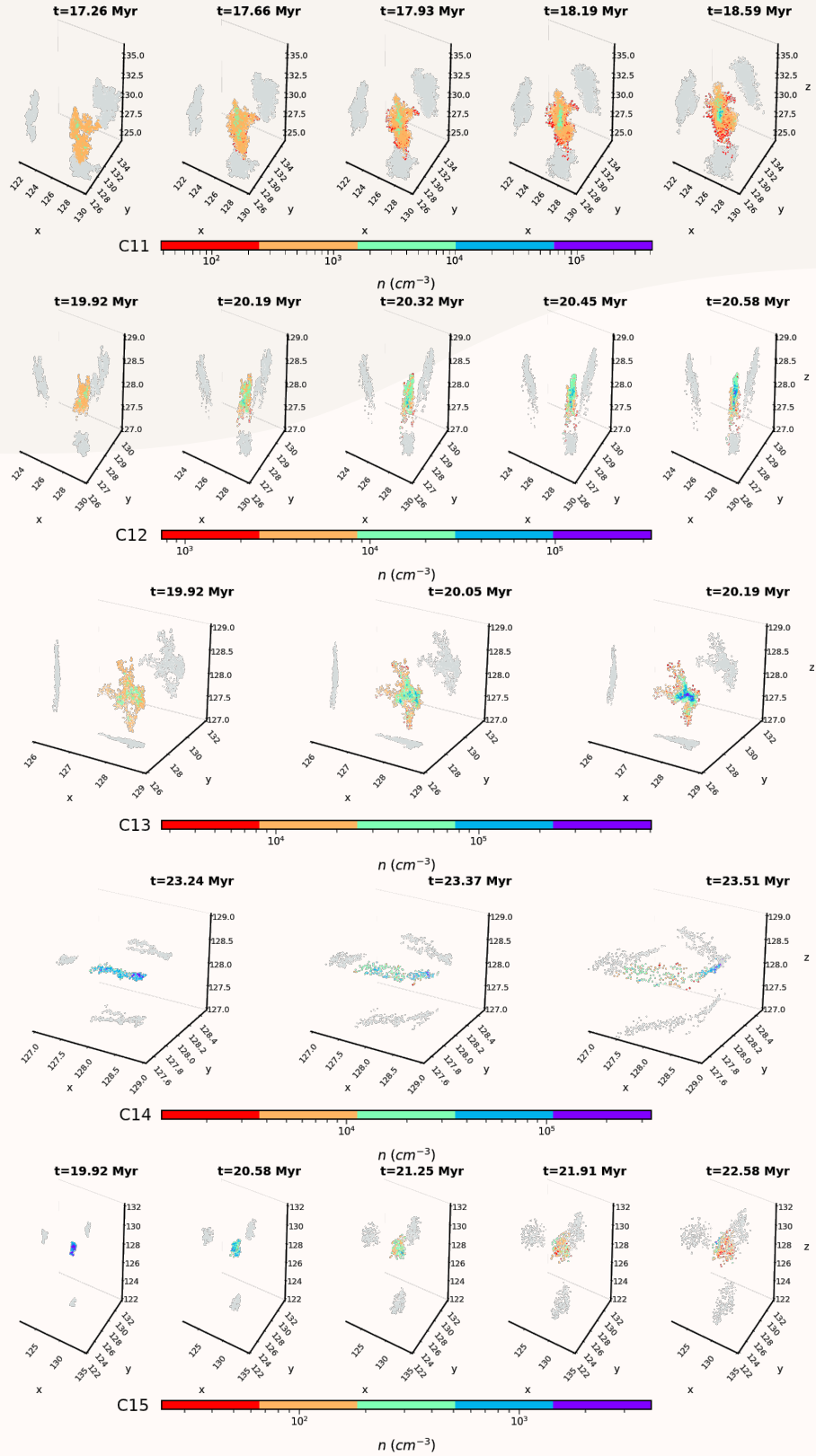


Figure 7: Density and spatial distribution evolution of the set of member particles of five clumps defined by density thresholds $n_{\text{th}} = 10^3 \text{ cm}^{-3}$ (C11), $n_{\text{th}} = 3 \times 10^3 \text{ cm}^{-3}$ (C12), $n_{\text{th}} = 10^4 \text{ cm}^{-3}$ (C13), $n_{\text{th}} = 3 \times 10^4 \text{ cm}^{-3}$ (C14), and $n_{\text{th}} = 10^3 \text{ cm}^{-3}$ (C15), at times $t_{\text{def}} = 17.26 \text{ Myr}$ (C11), $t_{\text{def}} = 19.92 \text{ Myr}$ (C12 and C13), and $t_{\text{def}} = 23.24 \text{ Myr}$ (C14 and C15). These clumps were tracked toward the future until they formed sinks. It can be seen that, for Clumps A-D, the innermost part of the particle set undergoes collapse, while the outermost particles decrease their density and appear to escape from the clump. Instead, Clump E turns out to be a transient clump that disperses as time passes.

It is important to note that the material that lowers its density and disperses can in some cases represent a significant fraction of the mass of the clump, and therefore, impose a limit on the SFE. To quantify this upper bound, in Fig. 9 we show the evolution, from t_{def} to the last snapshot before the formation of a sink, of the mass fraction below the indicated density for the lagrangian particle sets corresponding to clumps C11 to C14 from Fig. 7. These clumps were defined with a different density threshold each. It is seen from Fig. 9 that, for all four lagrangian sets, the mass fraction below the clump's defining threshold density increases monotonically in time, reaching $\sim 20\%$ of the total mass of the lagrangian set for C11 after 1.33 Myr, $\sim 5\%$ for C12 after 0.66 Myr, $\sim 5\%$ for C13 after 0.27 Myr, and $\sim 60\%$ for C14, also after 0.27 Myr. An analytical model is still necessary to establish whether the angular momentum transfer process sets any hard upper limits on the SFE. Some preliminary results regarding this issue are shown below.

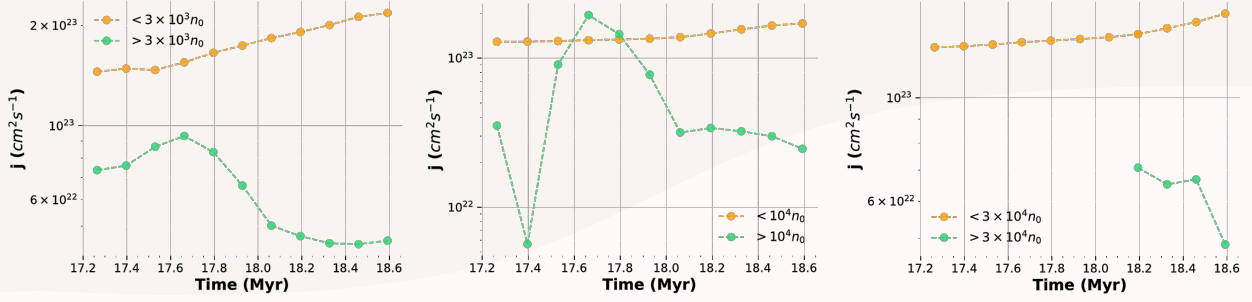


Figure 8: Evolution of the specific angular momentum j of the member particles of C11 (shown in Fig. 7) that are above and below the density thresholds $n_{\text{th}} = 3 \times 10^3$ (left column), 10^4 (middle column) and $3 \times 10^4 \text{ cm}^{-3}$ (right column). It can be seen that systematically the material below each of the three density thresholds studied contains most of the specific angular momentum of the clump.

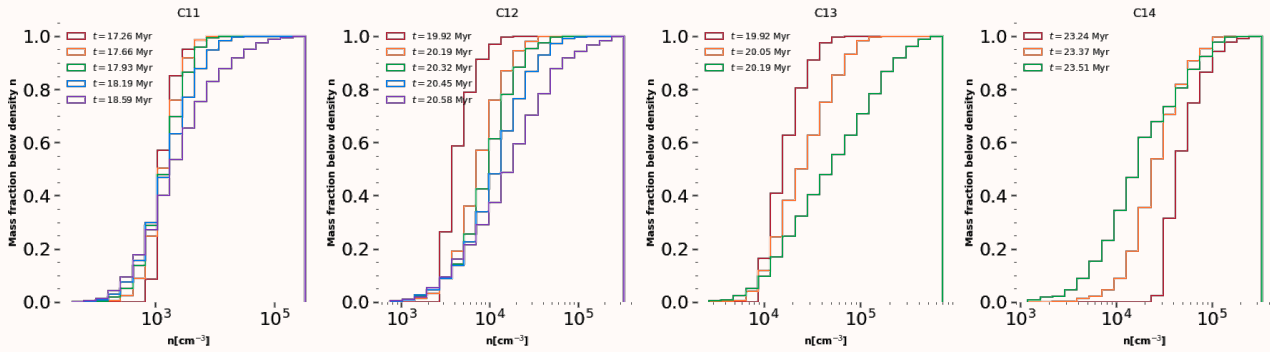


Figure 9: Evolution of the normalized cumulative density histogram for clumps C11 to C14 (shown in Fig. 7), respectively defined with density thresholds $n_{\text{th}} = 10^3 \text{ cm}^{-3}$ (C11), $n_{\text{th}} = 3 \times 10^3 \text{ cm}^{-3}$ (C12), $n_{\text{th}} = 10^4 \text{ cm}^{-3}$ (C13), and $n_{\text{th}} = 3 \times 10^4 \text{ cm}^{-3}$ (C14), at times $t_{\text{def}} = 17.26 \text{ Myr}$ for C11, $t_{\text{def}} = 19.92 \text{ Myr}$ for C12 and C13, and $t_{\text{def}} = 23.24$ for C14. It is seen that, at the final time (which represents the last snapshot prior to the formation of sinks) in the various cases, a fraction between ~ 5 and 60% of the mass acquires a density below the definition threshold density, so that only the remaining mass can continue to collapse.

Specific angular momentum evolution of a regular clump (always defined as a connected overdensity)

The second type of method for time tracking the clumps consists of defining them by means of a density threshold at each snapshot; that is, as connected sets of particles above a density thresh-

old throughout their evolution. This method was applied to clumps C16-C18 of Table 1. The general trend for these clumps is to grow in mass, size, and average density, due to accretion from their environment. The clumps are defined at a threshold $n_{\text{th}} = 3 \times 10^3 \text{ cm}^{-3}$ at times $t = 17.26$ (C16) and 17.93 Myr (C17 and C18). In Fig. 10 we show the evolution of these three clumps in the j - R diagram. For all three of them, the evolu-

tion in both radius and SAM occurs along evolutionary tracks close to the locus of the observational sample in this diagram. It is noteworthy that the evolution occurs towards *larger* radius and SAM, in spite of the clumps being in the process of collapse. Again, this is due to accretion from their environment.

In particular, this form of tracking is similar to the definition of clumps in observational samples. This suggests that the clumps that make up observational samples do not correspond to a sequence of objects that have contracted monolithically as a single unit, but rather constitute fragments of larger objects, which have managed to contract by transferring some of their AM to their neighboring fluid parcels by turbulent viscosity. That is, a process in which one part of the clump is lost, carrying AM with it, and allowing the remainder to contract.

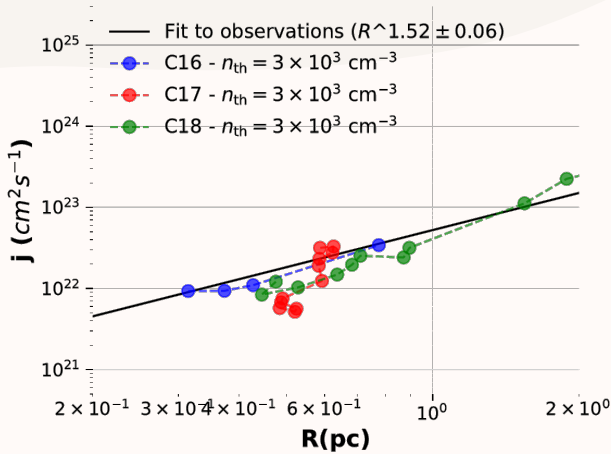


Figure 10: Specific angular momentum evolution of clumps C16-C18 (C16 is shown in Fig. ??), defined at times $t = 17.26$ (C16) and 17.93 (C17 and C18) as connected regions above $n_{th} = 3 \times 10^3 \text{ cm}^{-3}$, each one tracked until it forms sinks. The black line represents the slope of the fit to the observational data shown in Fig. 1.

Interpreting the results

The AM transfer mechanism

We have seen previously how the presence of the intruder particles is an important ingredient in the recovery of the observed j - R relation. This was seen in the lagrangian sets tracked from the past, which evolve with a slope close to the locus of the observations in the j - R diagram when the intruder particles represent a non-negligible fraction of the total mass. This is even more evident in the clumps tracked as connected sets above a density threshold at each time step, which are free to grow in mass and acquire AM from their surroundings as they accrete.

Since AM appears to be transported locally between adjacent particle layers instead of through a long-distance mechanism, the form of AM exchange seems to correspond to hydrodynamic torques exerted through turbulent (eddy) viscosity, rather than through (or, at least, in addition to) the gravitational torques suggested by Larson (1984) and Jappsen et al. (2005). These torques are exerted by shearing and compressive (in general, turbulent) stresses among the fluid parcels, as well as by the thermal pressure gradient described by the first and second terms on the right-hand side of eq. [1]).

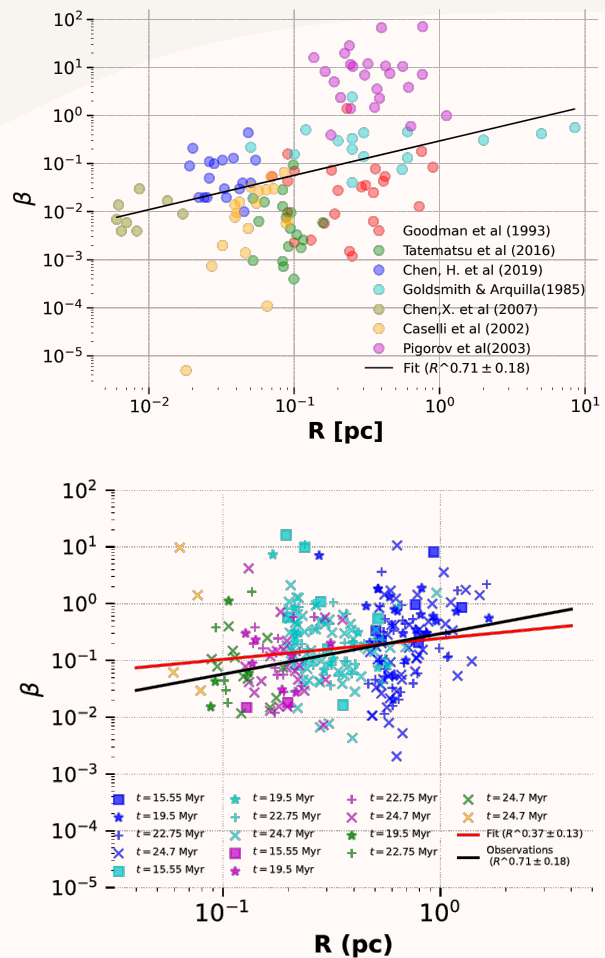


Figure 11: Top panel: β , the ratio of the rotational to the gravitational energy, vs. the radius R , for the observational sample. The black line represents a least squares fit to these data. Bottom panel: The same plot for the numerical sample. The black and red lines respectively represent the fits to the observational and the numerical data. Given the large scatter, the two samples appear to have very similar distributions.

In addition, since not all of a clump's particles par-

ticipate in the collapse, and instead a part of it is dispersed, it appears that the redistribution of AM occurs in a manner similar to that in accretion disks: if the whole object is subject to its self-gravity at all times, but prevented from contraction by the net rotation, then any local loss of AM in some subregion will allow it to contract, at the expense of transferring it to the rest of the parent structure. In the light of this new

result, we suggest that it is incorrect to think of a dense core as the result of the monolithic gravitational contraction of a larger clump, a process which should conserve AM. Instead, we suggest that the objects making up the observational data in Fig. 1 are precisely the *fragments* of larger structures that had to lose AM in the past to be able to contract.

Analytical estimates

In addition to the measurements described above in the simulation data, in AV21 we performed some simple calculations providing some insight about the possible origin of the j - R relation and the constancy of β , summarized below.

A plausible origin for the j - R scaling

We can perform a calculation similar to that of [Goodman et al. \(1993\)](#), but without assuming Larson's velocity dispersion-size relation as they did, and instead using the gravitational energy directly. We start by explicitly writing β as the ratio of the rotational to gravitational energies, both per unit mass, denoted by e_r and e_g . Noting that $e_r \approx (1/2)I\omega^2/M \approx (1/2)j\omega$ and $e_g \approx GM/R = \pi GR\Sigma$, where ω is a representative angular velocity for the clump and $\Sigma \approx M/\pi R^2$, we have

$$\beta \equiv \frac{e_r}{e_g} \approx \frac{1/2 j \omega}{\pi GR \Sigma}. \quad (7)$$

Following [Goodman et al. \(1993\)](#), under the assumption that $\beta \approx \text{cst.}$, we can then solve for ω as

$$\omega \approx \frac{2\pi\beta GR \Sigma}{j}. \quad (8)$$

On the other hand, the SAM is $j = I\omega/M \approx R^2\omega$. Substituting eq. (8) in this expression for j , we finally get

$$j \approx (2\pi\beta G \Sigma)^{1/2} R^{3/2}, \quad (9)$$

so that in the context of the GHC scenario (with all the structures dominated by self-gravity), we recover the dependence of j on R , as long as Σ does not vary much. This appears qualitatively analogous to the generalization of the Larson relations to the single scaling proposed by [Heyer et al. \(2009\)](#).

Constancy of β

A crucial assumption in the derivation above for the j - R scaling is that $\beta \sim \text{cst.}$, or at least that it does not depend on R . Here we outline a possible mechanism for this behavior. Let us assume that all regions larger than the Jeans length are attempting to contract due to the domination of self-gravity, and consider a region of fixed mass M . Its gravitational energy per unit mass, e_g , then, scales with radius as

$$e_g \approx \frac{GM}{R} \propto R^{-1}, \quad (10)$$

while its specific rotational energy is

$$e_r \approx \frac{1}{2} \frac{I\omega^2}{M} \approx \frac{1}{2} v_{\text{rot}}^2. \quad (11)$$

On the other hand, if the AM is conserved during the contraction,

$$J \approx \text{cst.} \approx I\omega \approx MR^2 \frac{v_{\text{rot}}}{R} = MRv_{\text{rot}}, \quad (12)$$

implying that $v_{\text{rot}} \propto R^{-1}$, and therefore

$$e_r \propto R^{-2}. \quad (13)$$

We thus see that, as a fluid parcel contracts due to gravity, the ratio of its rotational energy to its gravitational energy β would tend to increase, if its AM were conserved. This fact is also described by [Hennebelle et al. \(2013\)](#). This could only continue until $e_r \sim e_g$, at which point the collapse should be halted by rotation. However, if the parcel sheds its AM via turbulent torques, then the contraction can continue. It thus seems plausible that the competition between these two processes tends to keep β approximately constant, or at least, independent of radius.

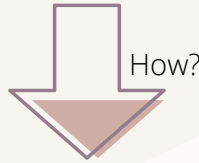
Pending work

Note: The numbering of pending tasks corresponds to the numbering of the Goals

Derived from AV21

2

Generate an analytical model for estimating the upper bound on star formation efficiency assuming that all structures are dominated by gravity and have an approximately constant rotational to gravitational energy ratio β .



Upper limit to the SFE

The fraction of the cloud mass that can collapse is the one that loses AM, so that the “efficiency” of the passage from a lower to a higher density, defined as the fraction of the clump mass that can reach that final density, can be determined by the condition that the amount of AM transferred allows the contracted clump to keep β constant. In this respect, we have performed the following preliminary calculation. Considering a parent cloud of mass M_p which in turn contains a fragment of mass M_f , the masses that satisfy the eq. (9) are respectively

$$M_p = \frac{j_p^2}{2pq\beta GR_p}; \quad (14)$$

$$M_f = \frac{j_f^2}{2pq\beta GR_f}. \quad (15)$$

Dividing equation (14) by equation (15), writing the radii of both the parent cloud and the fragment in terms of their densities, and defining the efficiency as $\epsilon = M_f/M_p$, we obtain

$$\epsilon \equiv \frac{M_{\rho_2}}{M_{\rho_1}} = \left(\frac{j_f}{j_p} \right)^{3/2} \delta^{1/4}, \quad (16)$$

where $\delta = \rho_f/\rho_p$, is the contrast in densities between the parent cloud and the fragment. This result shows that there is a family of possible configurations that the fragment can adopt to satisfy equation (9) given by the ratio of the parent and fragment radii. It is worth mentioning that [Hennebelle et al. \(2013\)](#) performed an analytical calculation on the energy variations between two rings of an accretion disk that exchange AM and mass, showing that the material tends to concentrate in the center and the angular momentum is expelled outwards. As a next task we plan to transport this idea to spherical shells to model this transport of mass and AM in molecular clouds, extending the calculation for the SFE as well.

3

Search for column density dependence of the j - R scaling relation.

How?

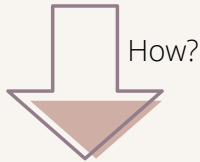


Equation (9) implies a generalization of the j - R scaling relation similar to that given to the Larson relations by the [Heyer et al. \(2009\)](#) scaling, so that $j \propto (\Sigma R^3)^{1/2}$, rather than scaling as $R^{3/2}$ alone. We plan to search for this relation both numerically and observationally, by sorting our observational and numerical samples by constant-column density subsets.

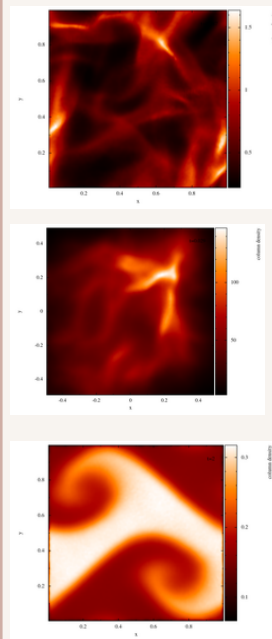
New simulations

4

Investigate the precise role of gravity in the generation of the j - R relation, the constancy of β , and the AM transfer mechanism by comparing it in simulations without self-gravity.



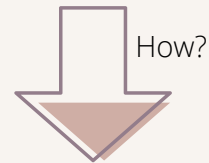
In the interpretation of AV21, self-gravity plays a fundamental role in the generation of the j - R relation and the independence of β on R , but not by generating tidal torques to exchange AM, as originally proposed by [Larson \(1984\)](#), but rather by driving gravitational contraction at all scales, while the AM transfer is due to turbulent viscous torques. To investigate the mechanism in detail, new numerical simulations will be carried out with the code PHANTOM ([Price et al., 2018](#)) analogous to the one studied in AV21, but without self-gravity, in order to determine whether the property of $\beta \approx \text{cst.}$ as well as the scaling j - Σ - R are preserved, or whether they take new forms in the absence of self-gravity. The PHANTOM code will replace the GADGET-2 code in the new simulations, as it will allow us to pass naturally to the magnetic case as explained in the next item. To date, the PHANTOM code is in the process of installation and compilation in two clusters at IRyA. At the same time, we have installed and compiled the code in our personal computers, and performed some tests with default setups. At this point we are generating our own setup to recreate the simulation studied in AV21 as a test.



Some screenshots of our experiments with the default setups

5

Investigate the role of the magnetic field by repeating the study of Arroyo-Chávez and Vázquez-Semadeni (2021, in press, hereafter AV21) in MHDSPH simulations using the code PHANTOM.



To maintain the possibility of individually tracking the clump particles in magnetic simulations, it is necessary to use SPH simulations that allow the incorporation of magnetic field. The code to use for this part of the project will be also the PHANTOM code. PHANTOM is a free parallel code for smoothed particle hydrodynamics and magnetohydrodynamics (SPH). With this code, a study similar to the one in AV21 will be carried out, with a set of simulations in which the intensity of the magnetic field is varied, and in which the particles that make up each clumps will be tracked both to the past and to the future to study the evolution of the SAM, and possible variations with respect to the non-magnetic case.

Collaborative work (extra)

The Density-Destiny plot

From the conference The Grand Cascade held in France this year, we are part of the project named “The Destiny-Density plot”. This collaboration seeks to determine the probability of a gas parcel of passing from one density to another; that is, the fraction of material in a certain region that increases or decreases its density with respect to a certain threshold in a certain time period. This provides an estimation of the fraction of the total gas that will participate in star formation over a certain time period. Applying mechanisms similar to those implemented in tracking our own clumps to the same SPH simulation, we present some preliminary results below.

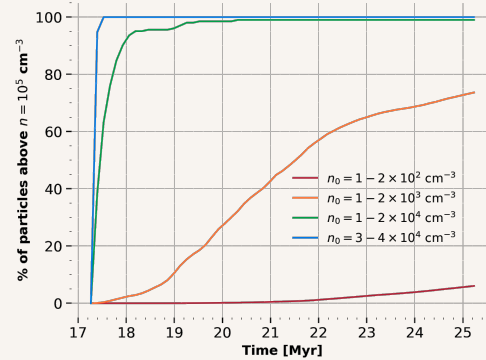
We took all the available particles in the numerical box within four density ranges at time 17.26 Myr in the simulation: 1,691,208 particles in $1-2 \times 10^2 \text{ cm}^{-3}$, 21,883 particles in $1-2 \times 10^3 \text{ cm}^{-3}$, 204 particles in $1-2 \times 10^4 \text{ cm}^{-3}$ and 38 particles in $3-4 \times 10^4 \text{ cm}^{-3}$. We have discarded all the particles that have previously fallen into a sink. We tracked these particles over ~ 8 Myr and computed the percentage of particles that reached densities $n > 10^5 \text{ cm}^{-3}$ and $n < 10^2 \text{ cm}^{-3}$ at the end of the test time.

The top panel in Fig. 12 shows the percentage of particles reaching $n_{\text{th}} > 10^5 \text{ cm}^{-3}$ at time t after being selected in the indicated initial density range. This shows that most of the particles with initial densities $> 10^3 \text{ cm}^{-3}$ reach the high density within this time period.

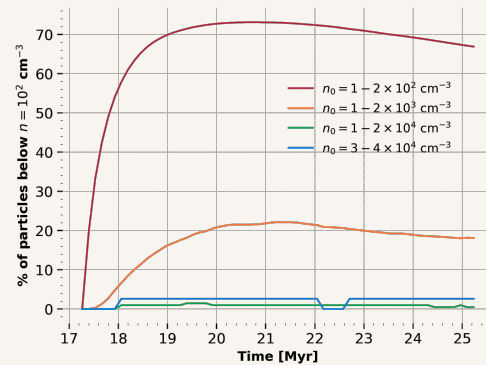
In the second panel of Fig. 12 we show the percentage of particles reaching $n_{\text{th}} < 100 \text{ cm}^{-3}$ at time t after being selected in the indicated initial density range. The fraction of particles initially just above 100 cm^{-3} which reaches $n < 100 \text{ cm}^{-3}$ rises rapidly and later begins to fall. This could be due to most of the particles in these ranges being initially in “voids” which are evacuated by the collapse onto distant centers. After some time they begin to fall themselves onto those centers and increase their density again.

The third and fourth panels in Fig. 12 are the density-destiny plots for the full sample of particles. For these plots we take the percentages of particles going below 100 cm^{-3} and above 10^5 cm^{-3} 8 Myr after having been selected from the indicated density range.

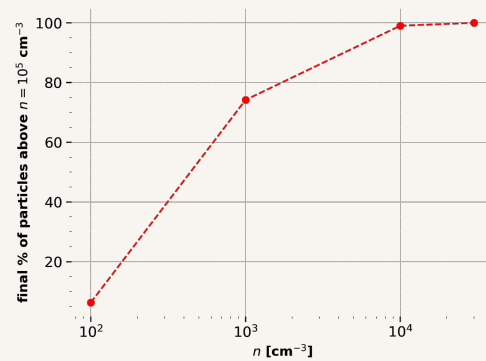
These preliminary results, although encouraging, have been performed in a simulation with no feedback. Repeating the procedure in simulations with feedback should give a more realistic estimation of the density-destiny plot, and therefore, of the net star formation efficiency for the gas.



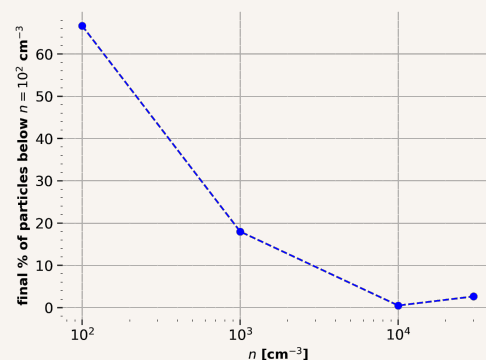
Percentage of particles reaching $n_{\text{th}} > 10^5 \text{ cm}^{-3}$ at time t after being selected in the indicated initial density range.



Percentage of particles reaching $n_{\text{th}} < 100 \text{ cm}^{-3}$ at time t after being selected in the indicated initial density range.



Density-Destiny plots for the sample of particles after 8 Myr for particles going above $n_{\text{th}} = 10^5 \text{ cm}^{-3}$.



Density-Destiny plots for the sample of particles after 8 Myr for particles going below $n_{\text{th}} = 10^2 \text{ cm}^{-3}$.

Figure 12: Density-Destiny plots

SCHEDULE

- Semester 1
 - Limit to star formation efficiency (in progress)
 - Planning of the PhD project
 - Beginning of the writing of the first article of the PhD (AV21)
- Semestre 2
 - Enlargement of the numerical sample to statistically justify the results of A20 and inclusion in article AV21
 - Sending article AV21 with increased numerical sample and increased observational sample (comparisons between both samples are still needed)
- Semester 3
 - Installation and familiarization with the code PHANTOM
 - Prepare and present the PhD candidate examn
 - Participation in the National Congress of Astronomy (Mexico) and From to Clouds to Discs (Dublin)
- Semester 4
 - Numerical simulation without selfgravity with PHANTOM to study the transport of angular momentum in the absence of selfgravity
 - Writing of the second PhD article on simulation without selfgravity.
 - Presentation in an international conference
- Semester 5
 - Numerical simulation with the code PHANTOM including magnetic fields: analysis of the effect of the magnetic field on the j - R relation
- Semester 6
 - Writing of the third PhD article corresponding to the magnetic case
 - Presentation in an international conference
 - Start of writing PhD thesis
- Semester 7
 - Thesis concluded and defense
- Semester 8
 - Semester left as margin for possible complications

Participation in conferences in this semester (recently added)

NEXT STEPS



REFERENCES

References

- Arroyo-Chávez, G. and Vázquez-Semadeni, E. (2021). Evolution of the angular momentum during gravitational fragmentation of molecular clouds. *arXiv e-prints*, page arXiv:2106.10381.
- Arroyo-Chávez, G. (2020). Evolución del momento angular específico durante el colapso y fragmentación de nubes moleculares. Tesis de maestría, IRyA UNAM.
- Ballesteros-Paredes, J., Hartmann, L. W., Vázquez-Semadeni, E., Heitsch, F., and Zamora-Avilés, M. A. (2011). Gravity or turbulence? Velocity dispersion-size relation. *A&AS*, 411(1):65–70.
- Bate, M. R. and Burkert, A. (1997). Resolution requirements for smoothed particle hydrodynamics calculations with self-gravity. *MNRAS*, 288(4):1060–1072.
- Bodenheimer, P. (1995). Angular Momentum Evolution of Young Stars and Disks. *ApJ*, 33:199–238.
- Camacho, V., Vázquez-Semadeni, E., Ballesteros-Paredes, J., Gómez, G. C., Fall, S. M., and Mata-Chávez, M. D. (2016). Energy Budget of Forming Clumps in Numerical Simulations of Collapsing Clouds. *MNRAS*, 833(1):113.
- Fleck, R. C., J. and Clark, F. O. (1981). A turbulent origin for the rotation of molecular clouds. *A&AS*, 245:898–902.
- Gaudel, M., Maury, A. J., Belloche, A., Maret, S., André, P., Hennebelle, P., Galametz, M., Testi, L., Cabrit, S., Palmeirim, P., Ladjelate, B., Codella, C., and Podio, L. (2020). Angular momentum profiles of Class 0 protostellar envelopes. *A&AS*, 637:A92.
- Goldsmith, P. F. and Arquilla, R. (1985). Rotation in dark clouds. In Black, D. C. and Matthews, M. S., editors, *Protostars and Planets II*, pages 137–149.
- Goodman, A. A., Benson, P. J., Fuller, G. A., and Myers, P. C. (1993). Dense Cores in Dark Clouds. VIII. Velocity Gradients. *A&AS*, 406:528.
- Hartmann, L. and Burkert, A. (2007). On the Structure of the Orion A Cloud and the Formation of the Orion Nebula Cluster. *A&AS*, 654(2):988–997.
- Heiner, J. S., Vázquez-Semadeni, E., and Ballesteros-Paredes, J. (2015). Molecular cloud formation as seen in synthetic H I and molecular gas observations. *A&AS*, 452(2):1353–1374.
- Hennebelle, P., Fromang, S., and Mathis, S. (2013). Angular momentum during star formation and early evolution. In Hennebelle, P. and Charbonnel, C., editors, *EAS Publications Series*, volume 62 of *EAS Publications Series*, pages 3–23.
- Heyer, M., Krawczyk, C., Duval, J., and Jackson, J. M. (2009). Re-Examining Larson’s Scaling Relationships in Galactic Molecular Clouds. *ApJ*, 699(2):1092–1103.
- Ibáñez-Mejía, J. C., Mac Low, M.-M., Klessen, R. S., and Baczynski, C. (2016). Gravitational Contraction versus Supernova Driving and the Origin of the Velocity Dispersion-Size Relation in Molecular Clouds. *A&AS*, 824(1):41.
- Imara, N. and Blitz, L. (2011). Angular Momentum in Giant Molecular Clouds. I. The Milky Way. *ApJ*, 732(2):78.
- Jappsen, A. K. and Klessen, R. S. (2004). Protostellar angular momentum evolution during gravoturbulent fragmentation. *A&AS*, 423:1–12.
- Jappsen, A. K., Klessen, R. S., Larson, R. B., Li, Y., and Mac Low, M. M. (2005). The stellar mass spectrum from non-isothermal gravoturbulent fragmentation. *A&AS*, 435(2):611–623.
- Koyama, H. and Inutsuka, S.-i. (2002). An Origin of Supersonic Motions in Interstellar Clouds. *ApJ*, 564(2):L97–L100.
- Kuznetsova, A., Hartmann, L., and Heitsch, F. (2019). The Origins of Protostellar Core Angular Momenta. *A&AS*, 876(1):33.
- Larson, R. B. (1981). Turbulence and star formation in molecular clouds. *A&AS*, 194:809–826.
- Larson, R. B. (1984). Gravitational torques and star formation. *A&AS*, 206:197–207.
- Li, Z. Y., Banerjee, R., Pudritz, R. E., Jørgensen, J. K., Shang, H., Krasnopolsky, R., and Maury, A. (2014). The Earliest Stages of Star and Planet Formation: Core Collapse, and the Formation of Disks and Outflows. In Beuther, H., Klessen, R. S., Dullemond, C. P., and Henning, T., editors, *Protostars and Planets VI*, page 173.
- Mouschovias, T. C. (1991). Single-Stage Fragmentation and a Modern Theory of Star Formation. In Lada, C. J. and Kylafis, N. D., editors, *The Physics of Star Formation and Early Stellar Evolution*, volume 342 of *NATO Advanced Study Institute (ASI) Series C*, page 449.

- Pineda, J. E., Zhao, B., Schmiedeke, A., Segura-Cox, D. M., Caselli, P., Myers, P. C., Tobin, J. J., and Dunham, M. (2019). The Specific Angular Momentum Radial Profile in Dense Cores: Improved Initial Conditions for Disk Formation. , 882(2):103.
- Price, D. J., Wurster, J., Tricco, T. S., Nixon, C., Toupin, S., Pettitt, A., Chan, C., Mentiplay, D., Laibe, G., Glover, S., Dobbs, C., Nealon, R., Liptai, D., Worpel, H., Bonnerot, C., Dipierro, G., Ballabio, G., Ragusa, E., Federrath, C., Iaconi, R., Reichardt, T., Forgan, D., Hutchison, M., Constantino, T., Ayliffe, B., Hirsh, K., and Lodato, G. (2018). Phantom: A Smoothed Particle Hydrodynamics and Magnetohydrodynamics Code for Astrophysics. , 35:e031.
- Shu, F. H., Adams, F. C., and Lizano, S. (1987). Star formation in molecular clouds: observation and theory. , 25:23–81.
- Spitzer, L. (1978). *Physical processes in the interstellar medium*.
- Vázquez-Semadeni, E., Gómez, G. C., Jappsen, A. K., Ballesteros-Paredes, J., González, R. F., and Klessen, R. S. (2007). Molecular Cloud Evolution. II. From Cloud Formation to the Early Stages of Star Formation in Decaying Conditions. , 657(2):870–883.
- Vázquez-Semadeni, E., Gómez, G. C., Jappsen, A. K., Ballesteros-Paredes, J., and Klessen, R. S. (2009). High- and Low-Mass Star-Forming Regions from Hierarchical Gravitational Fragmentation. High Local Star Formation Rates with Low Global Efficiencies. , 707(2):1023–1033.
- Vázquez-Semadeni, E., Palau, A., Ballesteros-Paredes, J., Gómez, G. C., and Zamora-Avilés, M. (2019). Global hierarchical collapse in molecular clouds. Towards a comprehensive scenario. , 490(3):3061–3097.